Supporting Information for: Thermo-compositional structure of the South American Platform lithosphere: Evidence of stability, modification and erosion.

Isabella Altoe[1], Saskia Goes[1], and Marcelo Assumpção[2]

[1]*Department of Earth Science and Engineering, Imperial College London, UK*
[2]*Department of Geophysics, IAG, University of São Paulo, São Paulo, Brazil*
Corresponding Author: i.altoe17@imperial.ac.uk

Contents of this file

1. Figures S1 to S16
2. Tables S1 to S5

Table S1 - Variability within the clusters to inter cluster distance

Cluster/Ave. distance to cluster	**C1**	**C2**	**C3**	**C4**	**C5**	**C6**
C1	0.0513	0.6220	0.2120	0.3704	0.2796	0.5156
C2	0.6120	0.0373	0.6046	0.3010	0.1294	0.1132
C3	0.1926	0.5991	0.0319	0.1319	0.3307	0.3474
C4	0.3478	0.2923	0.1287	0.0286	0.2015	0.1070
C5	0.2614	0.1252	0.3320	0.2060	0.0331	0.1297
C6	0.4849	0.0965	0.3362	0.0990	0.1172	0.0207

Average distance of the points in a cluster to every centroid for our preferred solution with six clusters. For six clusters, the within-cluster distance is lower than the distance between clusters. For more clusters, the average distances within and between clusters become similar.

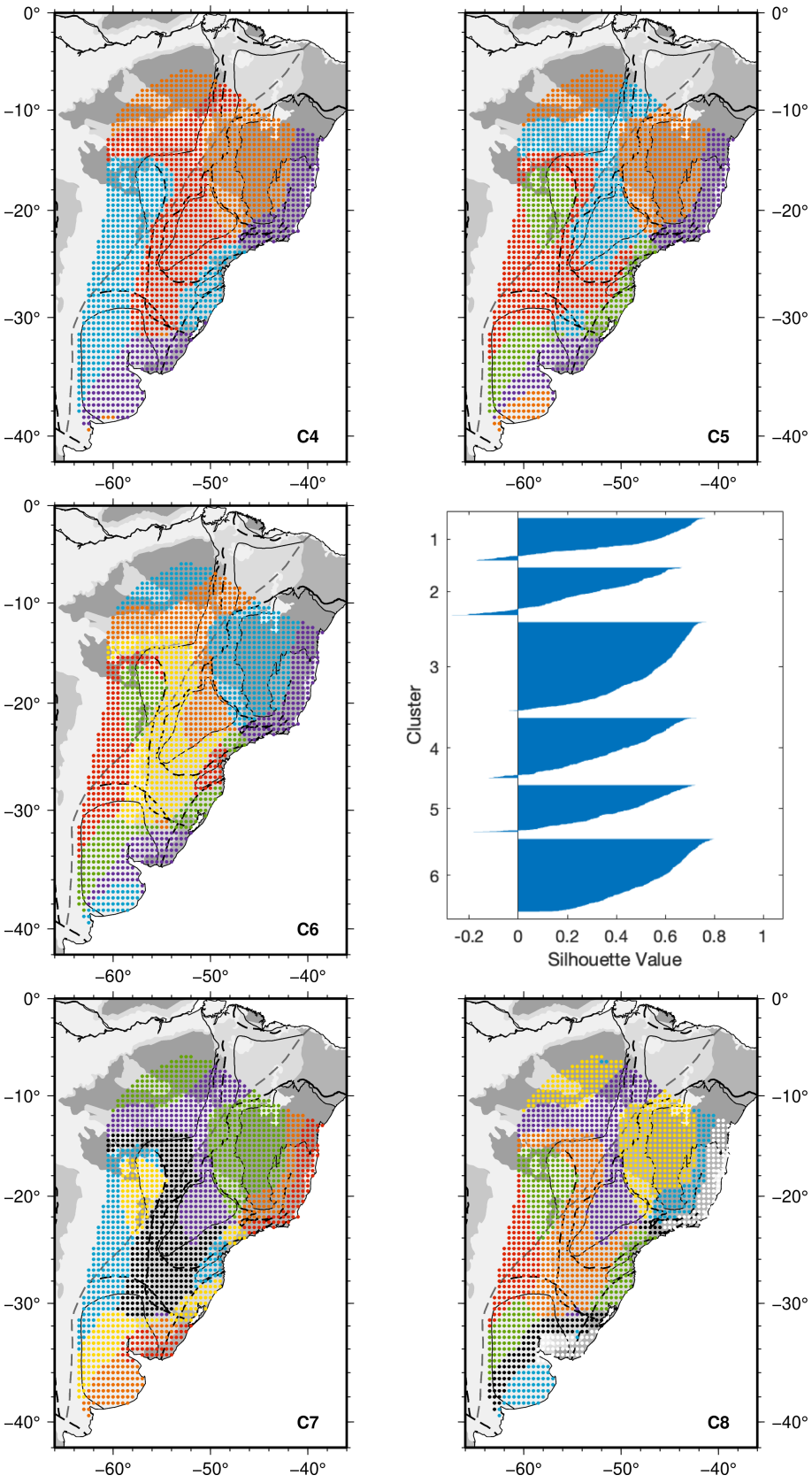

Figure S1 - Maps showing the k-means solutions for 4 to 8 clusters (labelled C4 through C8) and silhouette plot for 6 clusters. Each cluster generated by the cluster analysis is represented by one colour. On map C6, the black dots are the ones that have negative silhouette values and/or are geographic isolated and therefore were removed from further analysis.

Table S2 - Thermal Parameters

	Fixed parameters	**Value**	**Ref.**
k_c	Crustal thermal conductivity	2.7 $Wm^{-1}K^{-1}$	(Hasterok & Chapman, 2011; Michaut et al., 2007)
k_m	Mantle thermal conductivity	3.0 $Wm^{-1}K^{-1}$	(Hasterok & Chapman, 2011; Michaut et al., 2007)
A_{uc}	Upper crustal heat production	0.8 μWm^3	(Hasterok & Chapman, 2011; Michaut et al., 2007; Rudnick & Nyblade, 1999)
A_{lc}	Lower crustal heat production	0.4 μWm^3	(Hasterok & Chapman, 2011; Michaut et al., 2007; Rudnick & Nyblade, 1999)
A_m	Lithospheric mantle heat production	0.01 μWm^3	(Hasterok & Chapman, 2011; Michaut et al., 2007)
	Variable parameters	**Range** (increment)	**Ref.**
q_m	Moho heat flow	10-35 (1.0) mWm^{-2}	(Lévy & Jaupart, 2011; Shapiro et al., 2004)
T_{pot}	Mantle potential temperature	1100-1300 (50)°C	(Herzberg et al., 2007)
	Obtained parameters	**Range**	**Ref.**
q_s	Surface heat flow	31-62 mWm^{-2}	(Lévy & Jaupart, 2011; Shapiro et al., 2004)
L_T	Thermal lithospheric thickness	90-360 km	(Jaupart & Mareschal, 1999)

Crustal thickness for each group is given in Table S3 - Crustal Parameters

Table S3 - Crustal Parameters

Groups	H (km)	ρ_{uc} (kg/m^3)	ρ_{lc} (kg/m^3)	$V_{p\text{-}uc}$ (m/s)	$V_{s\text{-}uc}$ (m/s)	$V_{p\text{-}lc}$ (m/s)	$V_{s\text{-}lc}$ (m/s)
3AmC	36 - 40	2780	2910	6290	3640	6810	3850-4000
3SFC	37 - 41	2760	2970	6250	3580	7020	3950-4100
4PcB	38 - 42	2760	2920	6200	3570	6890	3900-4050
4PrB	42 - 46	2730	3000	6160	3520	7090	4000-4150
6PrB(n)	34 - 37	2760	2940	6260	3590	6950	3900-4050
6PrB(w)	39 - 43	2730	2980	6130	3500	7060	4000-4150
6PrB(s)	39 - 43	2750	2930	6110	3500	6920	3900-4050
5PtB	38 - 42	2740	2970	6240	3520	7015	3900-4050
2ChB	38 - 41	2700	2960	6100	3400	6990	3900-4050
2LAC	37 - 41	2760	2910	6230	3600	6800	3950-4000
5RPC	37 - 41	2730	2960	6130	3510	7000	3950-4100
3RPC	33 - 37	2700	2980	6030	3470	7070	4000-4150

Crustal parameters used for each group. H is crustal thickness, ρ is density, uc is upper crust, lc is lower crust, V_p is P-wave velocity, V_s is S-wave velocity. The depth of the upper-lower crust boundary is 2/3 of the crustal thickness. Groups: 3Amc (Amazonian Craton), 3SFC (São Francisco Craton), 4PcB (Parecis Basin), 4PrB (Paraná Basin), 6PrB(n) (Paraná Basin north), 6PrB(w) (Paraná Basin west), 6PrB(s) (Paraná Basin south), 5PtB (Pantanal Basin), 2ChB (Chaco Basin), 2LAC (Luiz Alves Craton), 5RPC (Rio de la Plata Craton), 3RPC (Rio de la Plata Craton) (see map in Fig. 3). Data from Rivadeneyra-Vera et al. (2019) and CRUST1.0 (Laske et al., 2013)

Table S4 - Compositions considered

Composition (wt%)	SiO_2	TiO_2	Al_2O_3	FeO	MnO	MgO	CaO	Na_2O	K_2O	H_2O
ARC9 (Dunite)	42.90	0.01	0.30	6.50	0.15	49.20	0.10	0.10		
ARC4 (lherzolite)	44.3	0.17	1.74	8.1	0.12	43.3	1.27	0.12		
Pyrolite	44.93	0.00	4.37	8.56		38.82	3.19	0.13		
MORB	50.6	1.5	15.7	10.6		7.6	11.1	2.6	0.2	
ARC9 with 0.215 wt% H2O	42.90	0.01	0.30	6.50		49.20	0.10	0.10		0.215
ARC9 with 5wt% phl	43.28	00.1	0.90	6.23		48.61	0.10	0.10	0.57	0.22

References: ARC9 and ARC4 from Griffin et al. (2009), Pyrolite from Xu et al. (2008), MORB from Hacker (2008).

Table S5 - Solid-solution models used

Abbreviation	Mineral	Ref.
Act(M)	low-pressure amphibole	(Massonne, 2008)
Atg(PN)	antigorite	(Padrón-Navarta et al., 2013)
Chl(HP)	chlorite	(T. Holland et al., 1998)
Cpx(HP)	clinopyroxene	(T. Holland & Powelll, 1996)
Ctd(HP)	chloritoid	(White et al., 2000)
GlTrTsPg	clinoamphibole	(Wei & Powell, 2003; White et al., 2003)
Gt(HP)	garnet	(T. J. Holland & Powell, 1998)
O(HP)	olivine	(T. J. Holland & Powell, 1998)
Opx(HP)	orthopyroxene	(T. Holland & Powelll, 1996)
Pl(h)	feldspar	(Newton et al., 1980)
Sp(JR)	spinel	(Jamieson & Roeder, 1984)
T	talc	ideal

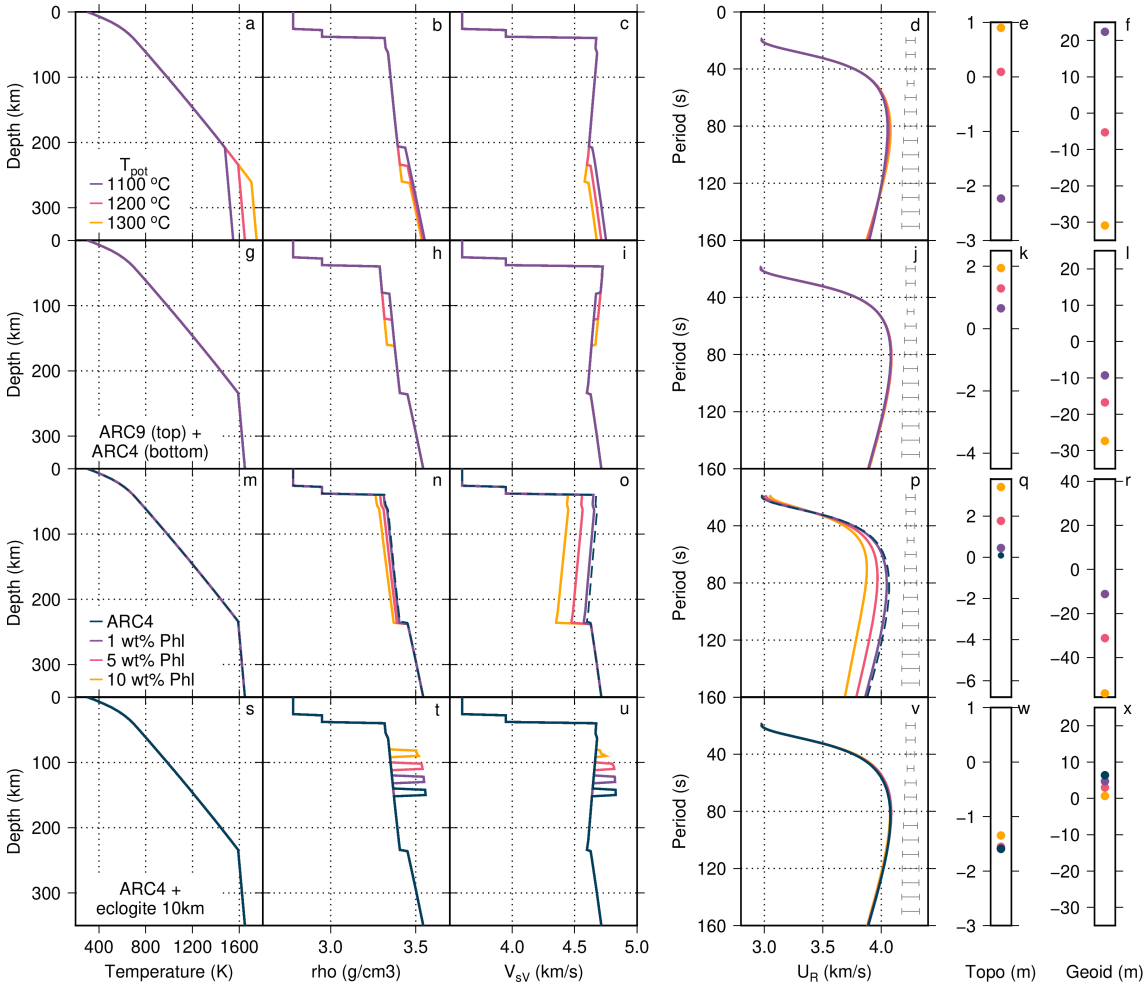

Figure S2 Sensitivity analysis of group Rayleigh-wave dispersion curves, topography, and geoid height to different mantle potential temperature (first row), layered background composition (second row), plhogopite content (third row), and a layer of eclogite at different depths (forth row) . For each set of tests, the left hand side shows the geotherms (a, g, m, and s), the density (b, h, n, and t) and the velocity profiles (c, i, o, and u). The right hand side shows the effect of the different thermal and compositional parameters to the group Rayleigh-wave dispersion curves (d, i, p, and v), topography (e, k, q, and w) and geoid (f, l, r, and x).

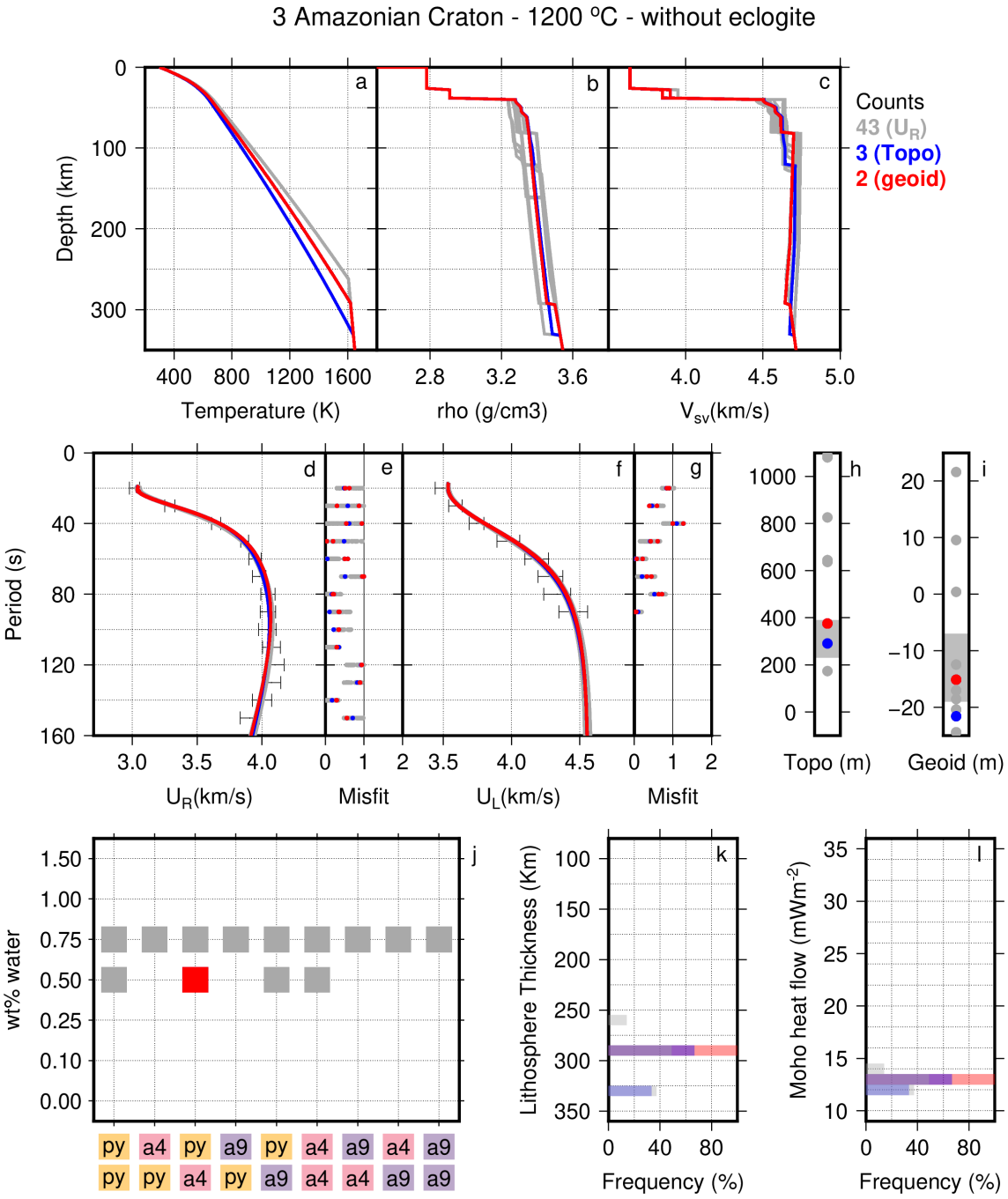

Figure S3 Set of solutions for group 3 Amazonian Craton (3AmC) for a sublithospheric potential temperature of 1200°C without an eclogitic layer. All solutions that fit the dispersion curves are in grey; those that fit both the dispersion curves and the elevation are in blue; those that fit dispersion curves, elevation, and geoid are in red. Top row: (a) Geotherms, (b) density profiles, and (c) V_{SV} profiles. Middle row: (d) group Rayleigh-wave groups velocities vs period and, (e) respective misfits, (f) group Love-wave groups velocities vs period. and (g) respective misfits, (h) and (i) show elevation and geoid, respectively, with a dark grey box for the observed range. Bottom row: (j) water content vs background composition (top layer/bottom layer), (k) and (l) show histograms of the solutions for thermal lithosphere thickness, and Moho heat flow.

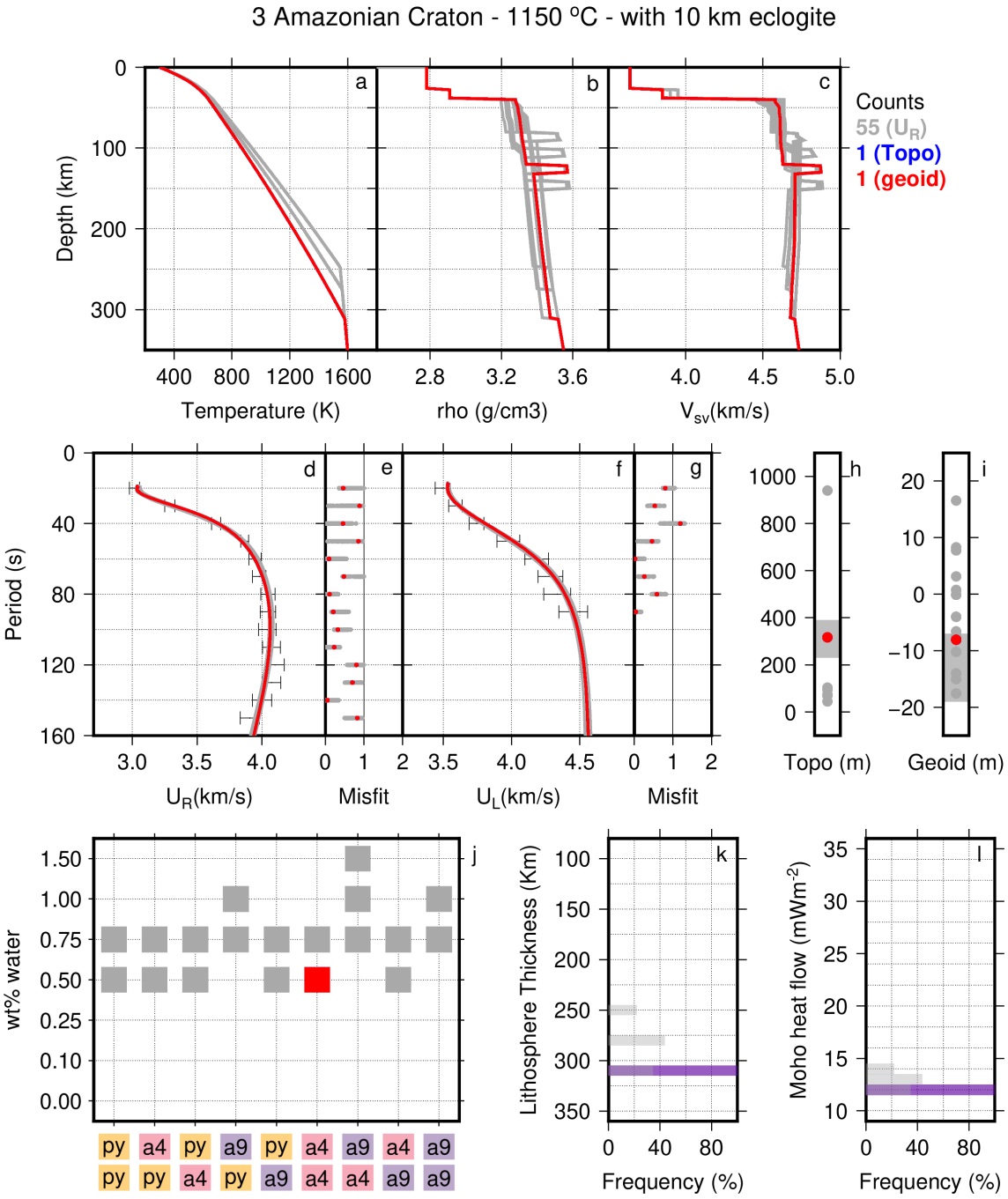

Figure S4 Set of solutions for group 3 Amazonian Craton (3AmC) for a sublithospheric potential temperature of 1150°C with a 10 km eclogitic layer. All solutions that fit the dispersion curves are in grey; those that fit both the dispersion curves and the elevation are in blue; those that fit dispersion curves, elevation, and geoid are in red. Top row: (a) Geotherms, (b) density profiles, and (c) V_{SV} profiles. Middle row: (d) group Rayleigh-wave groups velocities vs period and, (e) respective misfits, (f) group Love-wave groups velocities vs period. and (g) respective misfits, (h) and (i) show elevation and geoid, respectively, with a dark grey box for the observed range. Bottom row: (j) water content vs background composition (top layer/bottom layer), (k) and (l) show histograms of the solutions for thermal lithosphere thickness, and Moho heat flow.

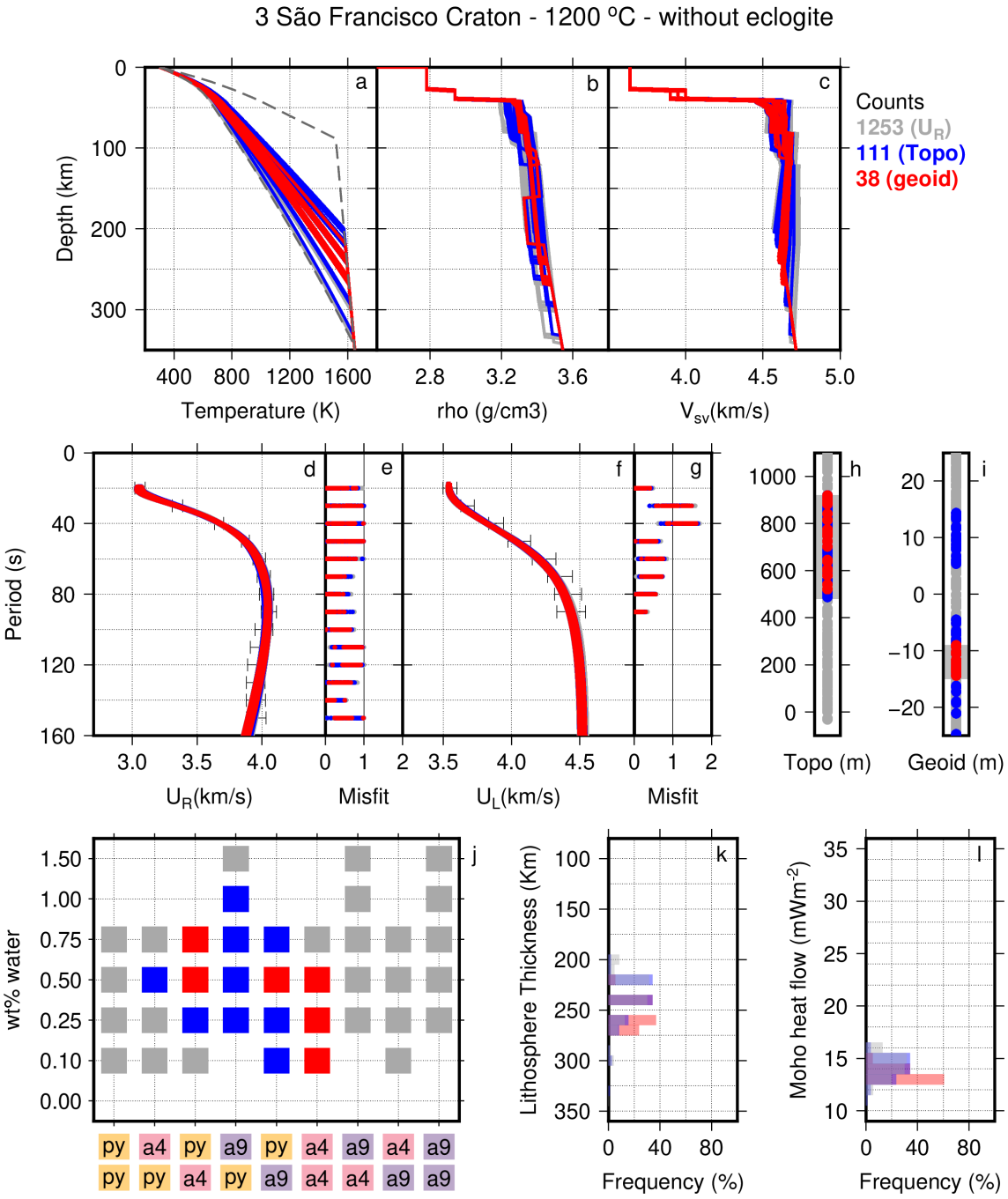

Figure S5 Set of solutions for group 3 São Francisco Craton (3SFC) for a sublithospheric potential temperature of 1200°C without an eclogitic layer. All solutions that fit the dispersion curves are in grey; those that fit both the dispersion curves and the elevation are in blue; those that fit dispersion curves, elevation, and geoid are in red. Top row: (a) Geotherms, (b) density profiles, and (c) V_{SV} profiles. Middle row: (d) group Rayleigh-wave groups velocities vs period and, (e) respective misfits, (f) group Love-wave groups velocities vs period. and (g) respective misfits, (h) and (i) show elevation and geoid, respectively, with a dark grey box for the observed range. Bottom row: (j) water content vs background composition (top layer/bottom layer), (k) and (l) show histograms of the solutions for thermal lithosphere thickness, and Moho heat flow.

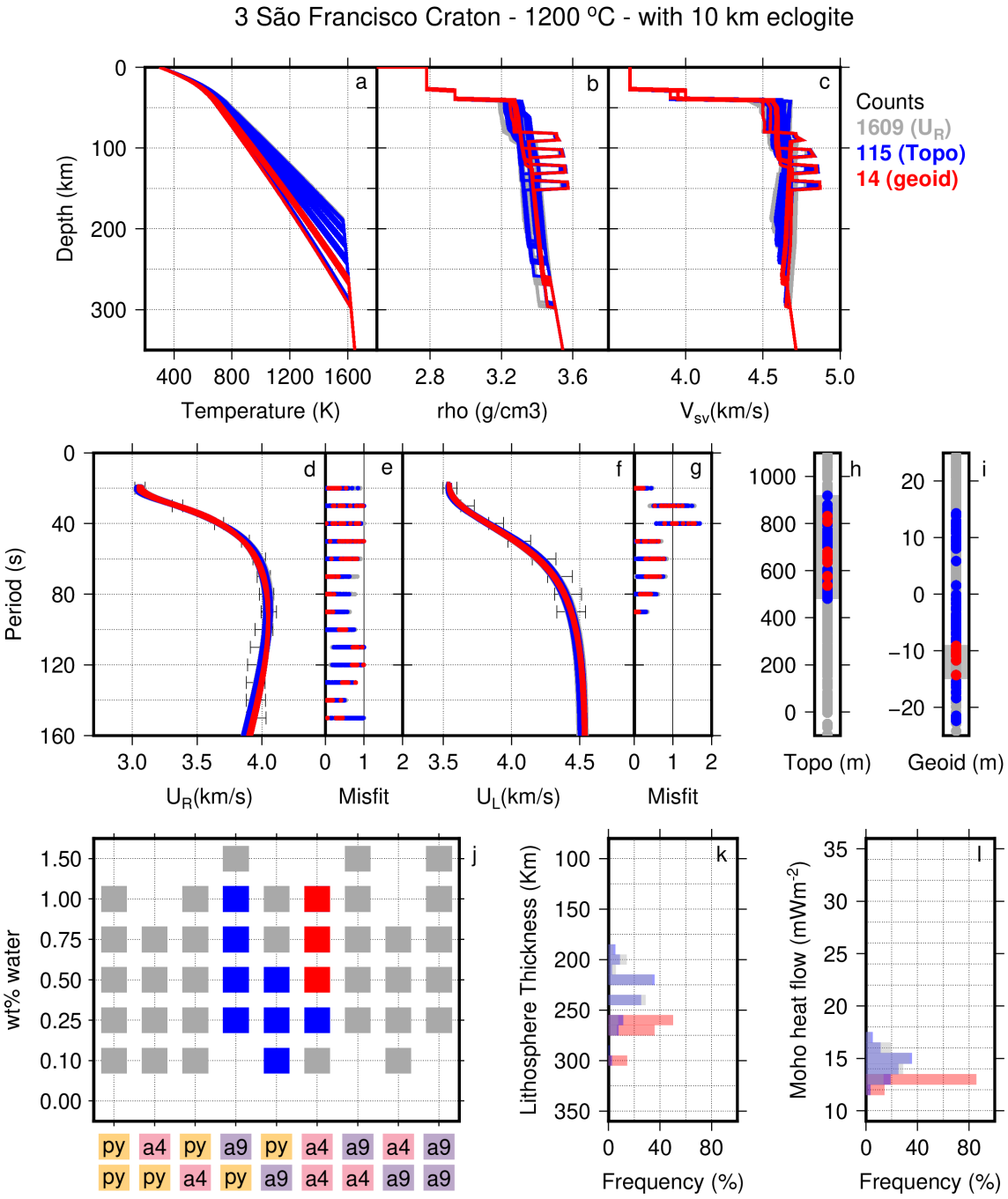

Figure S6 Set of solutions for group 3 São Francisco Craton (3SFC) for a sublithospheric potential temperature of 1200°C wit a 10 km eclogitic layer. All solutions that fit the dispersion curves are in grey; those that fit both the dispersion curves and the elevation are in blue; those that fit dispersion curves, elevation, and geoid are in red. Top row: (a) Geotherms, (b) density profiles, and (c) V_{SV} profiles. Middle row: (d) group Rayleigh-wave groups velocities vs period and, (e) respective misfits, (f) group Love-wave groups velocities vs period. and (g) respective misfits, (h) and (i) show elevation and geoid, respectively, with a dark grey box for the observed range. Bottom row: (j) water content vs background composition (top layer/bottom layer), (k) and (l) show histograms of the solutions for thermal lithosphere thickness, and Moho heat flow.

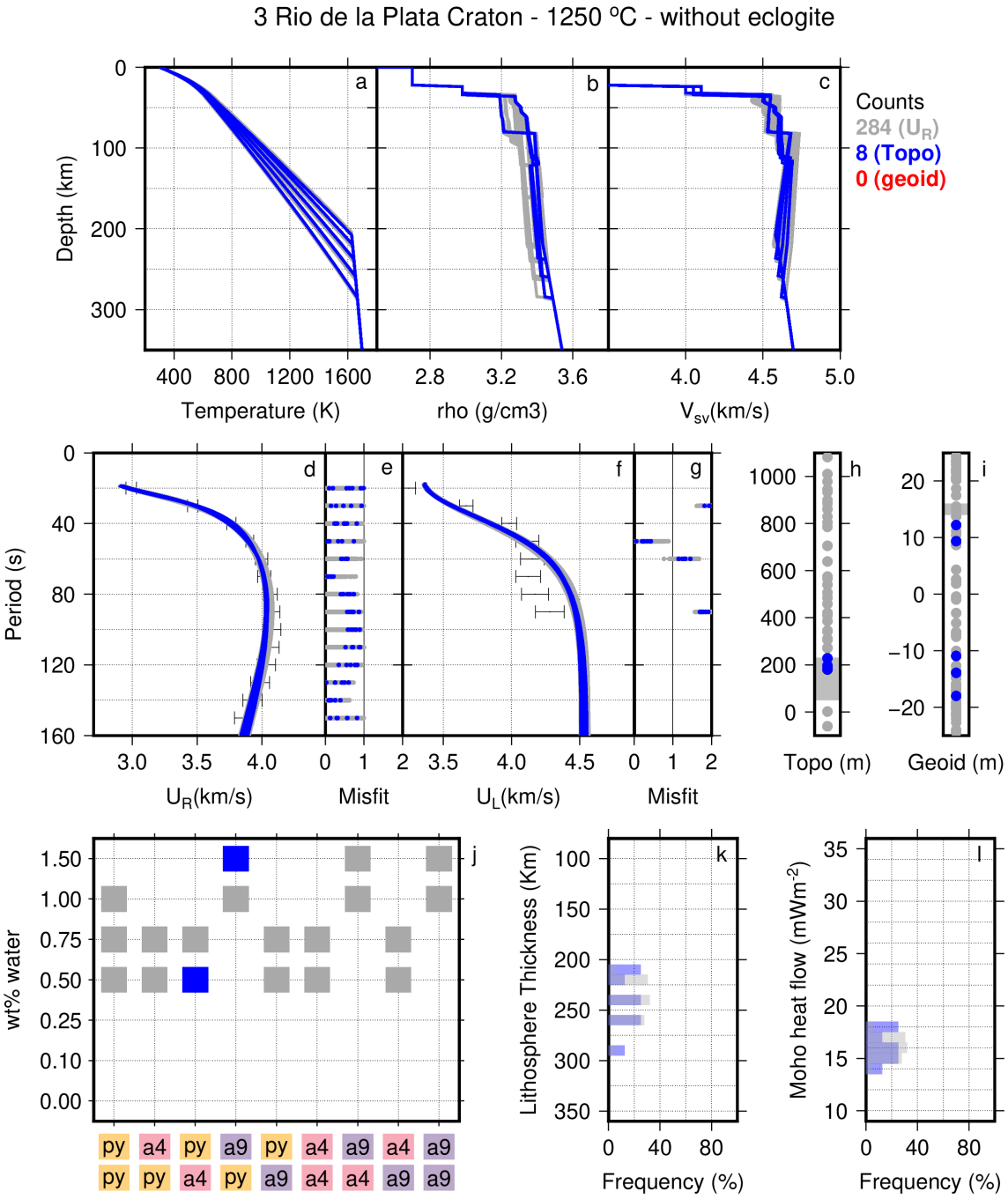

Figure S7 Set of solutions for group 3 Rio de la Plata Craton (3RPC) for a sublithospheric potential temperature of 1250°C without an eclogitic layer. All solutions that fit the dispersion curves are in grey; those that fit both the dispersion curves and the elevation are in blue; those that fit dispersion curves, elevation, and geoid are in red. Top row: (a) Geotherms, (b) density profiles, and (c) V_{SV} profiles. Middle row: (d) group Rayleigh-wave groups velocities vs period and, (e) respective misfits, (f) group Love-wave groups velocities vs period. and (g) respective misfits, (h) and (i) show elevation and geoid, respectively, with a dark grey box for the observed range. Bottom row: (j) water content vs background composition (top layer/bottom layer), (k) and (l) show histograms of the solutions for thermal lithosphere thickness, and Moho heat flow.

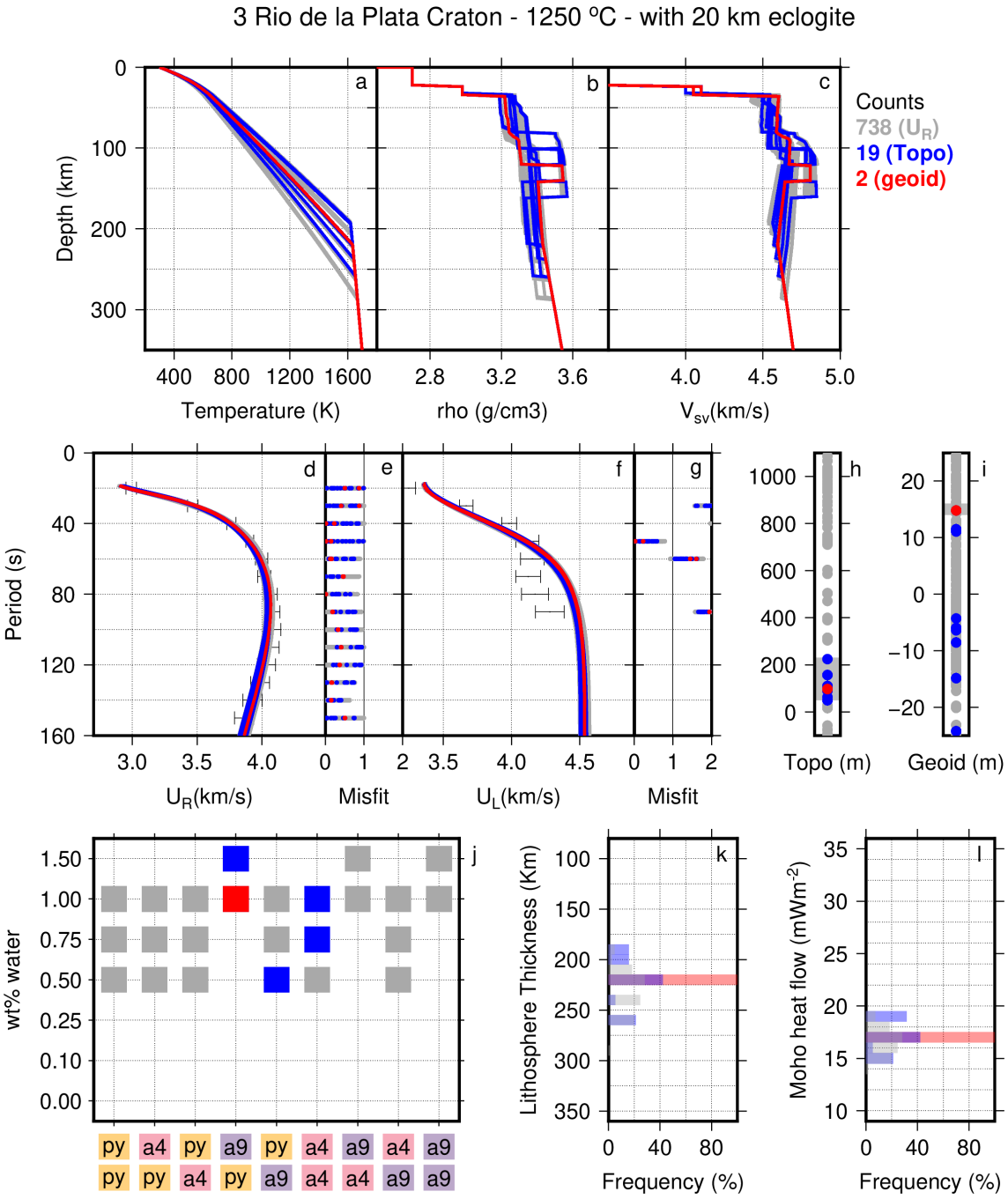

Figure S7 Set of solutions for group 3 Rio de la Plata Craton (3RPC) for a sublithospheric potential temperature of 1250°C with a 20 km eclogitic layer. All solutions that fit the dispersion curves are in grey; those that fit both the dispersion curves and the elevation are in blue; those that fit dispersion curves, elevation, and geoid are in red. Top row: (a) Geotherms, (b) density profiles, and (c) V_{SV} profiles. Middle row: (d) group Rayleigh-wave groups velocities vs period and, (e) respective misfits, (f) group Love-wave groups velocities vs period. and (g) respective misfits, (h) and (i) show elevation and geoid, respectively, with a dark grey box for the observed range. Bottom row: (j) water content vs background composition (top layer/bottom layer), (k) and (l) show histograms of the solutions for thermal lithosphere thickness, and Moho heat flow.

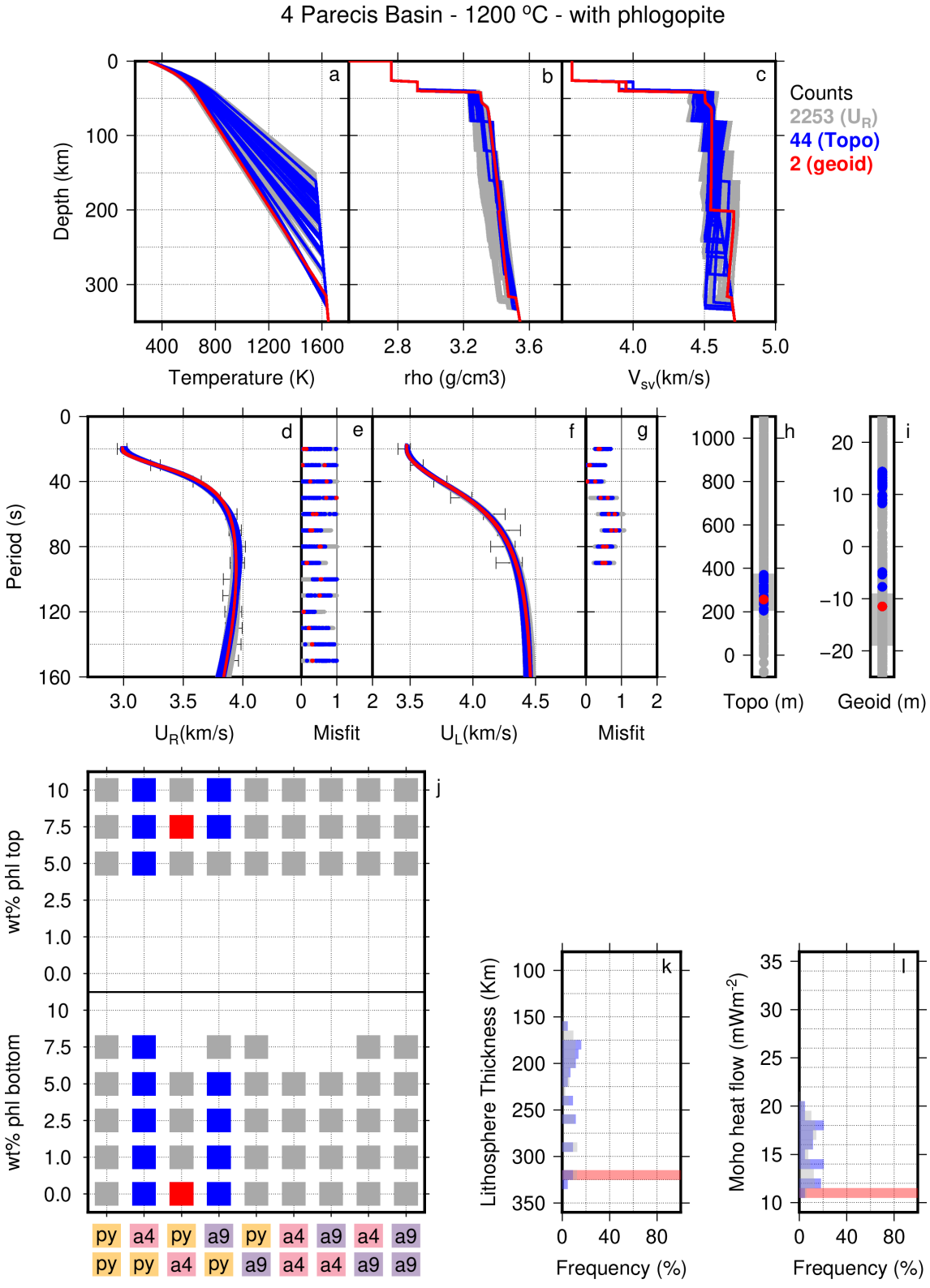

Figure S8 Set of solutions for group 4 Parecis Basin (4PcB) for a sublithospheric potential temperature of 1200°C with addition of Plogopite. All solutions that fit the dispersion curves are in grey; those that fit both the dispersion curves and the elevation are in blue; those that fit dispersion curves, elevation, and geoid are in red. Top row: (a) Geotherms, (b) density profiles, and (c) V_{SV} profiles. Middle row: (d) group Rayleigh-wave groups velocities vs period and, (e) respective misfits, (f) group Love-wave groups velocities vs period. and (g) respective misfits, (h) and (i) show elevation and geoid, respectively, with a dark grey box for the observed range. Bottom row: (j) Phlogopite content vs background composition (top layer/bottom layer), (k) and (l) show histograms of the solutions for thermal lithosphere thickness, and Moho heat flow.

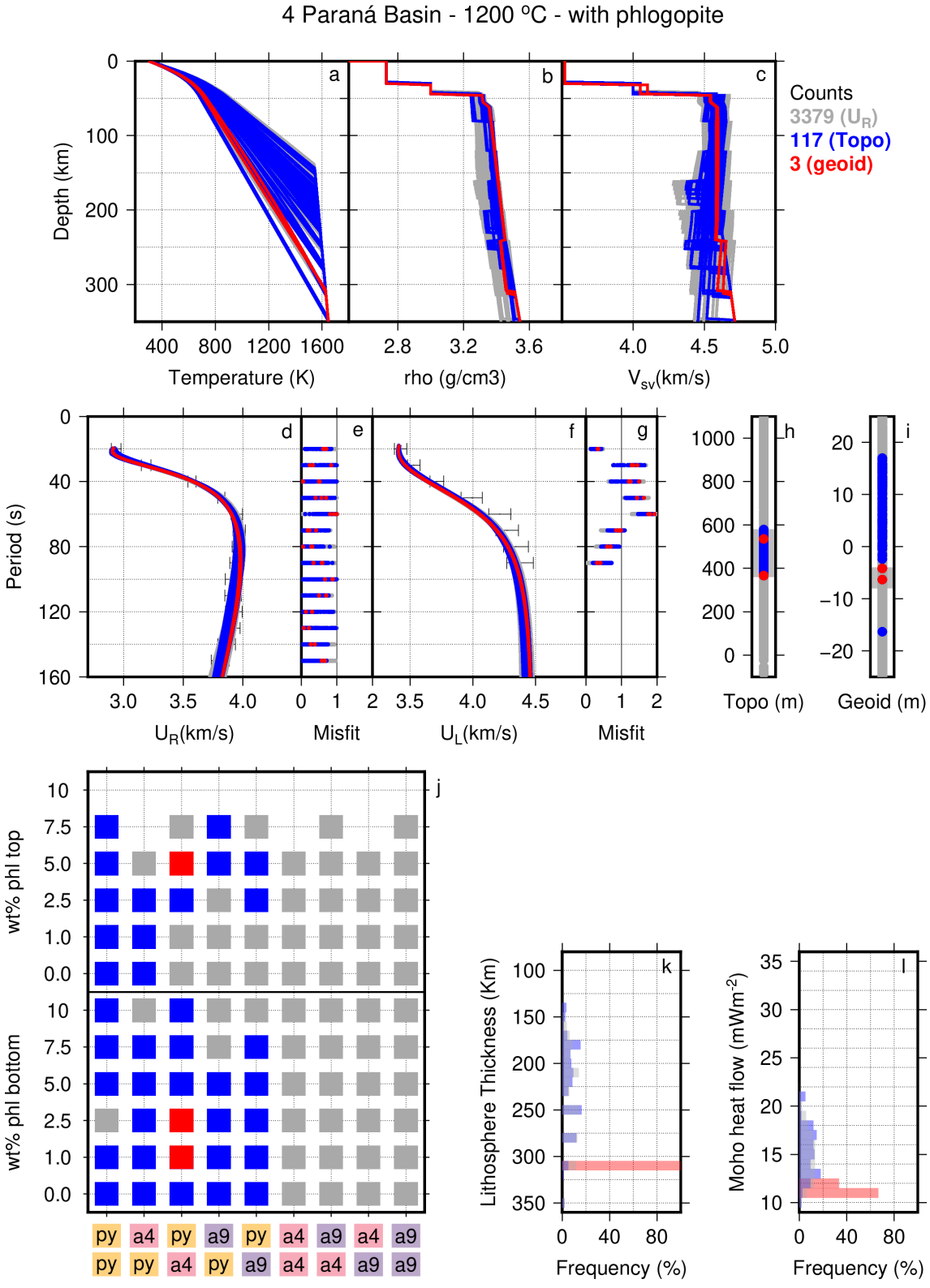

Figure S9 Set of solutions for group 4 Paraná Basin (4PrB) for a sublithospheric potential temperature of 1200°C with addition of Plogopite. All solutions that fit the dispersion curves are in grey; those that fit both the dispersion curves and the elevation are in blue; those that fit dispersion curves, elevation, and geoid are in red. Top row: (a) Geotherms, (b) density profiles, and (c) V_{SV} profiles. Middle row: (d) group Rayleigh-wave groups velocities vs period and, (e) respective misfits, (f) group Love-wave groups velocities vs period. and (g) respective misfits, (h) and (i) show elevation and geoid, respectively, with a dark grey box for the observed range. Bottom row: (j) Phlogopite content vs background composition (top layer/bottom layer), (k) and (l) show histograms of the solutions for thermal lithosphere thickness, and Moho heat flow.

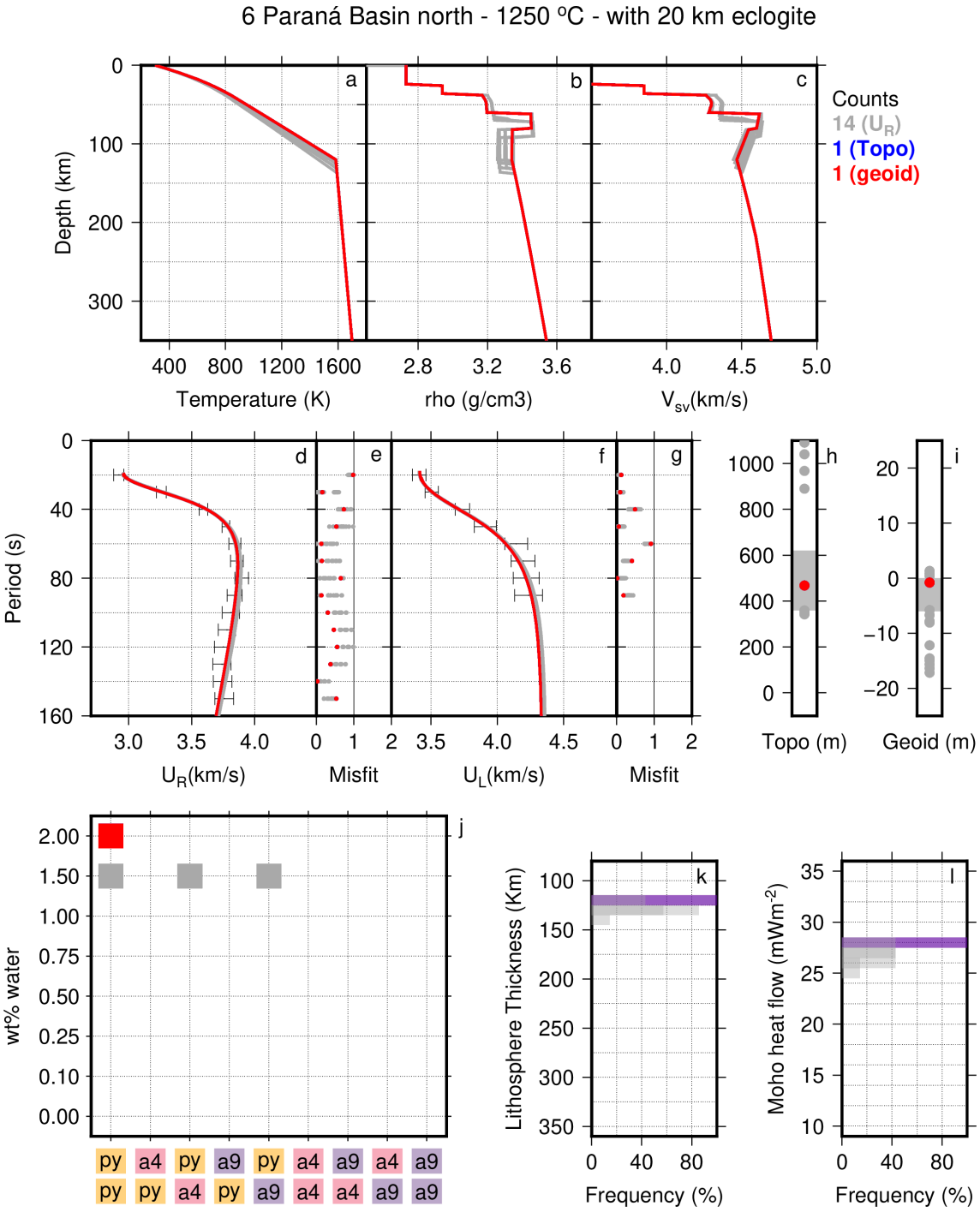

Figure S10 Set of solutions for group 6 Paraná Basin north (6PrB(n)) for a sublithospheric potential temperature of 1250°C with a 20 km eclogitic layer. All solutions that fit the dispersion curves are in grey; those that fit both the dispersion curves and the elevation are in blue; those that fit dispersion curves, elevation, and geoid are in red. Top row: (a) Geotherms, (b) density profiles, and (c) V_{SV} profiles. Middle row: (d) group Rayleigh-wave groups velocities vs period and, (e) respective misfits, (f) group Love-wave groups velocities vs period. and (g) respective misfits, (h) and (i) show elevation and geoid, respectively, with a dark grey box for the observed range. Bottom row: (j) water content vs background composition (top layer/bottom layer), (k) and (l) show histograms of the solutions for thermal lithosphere thickness, and Moho heat flow.

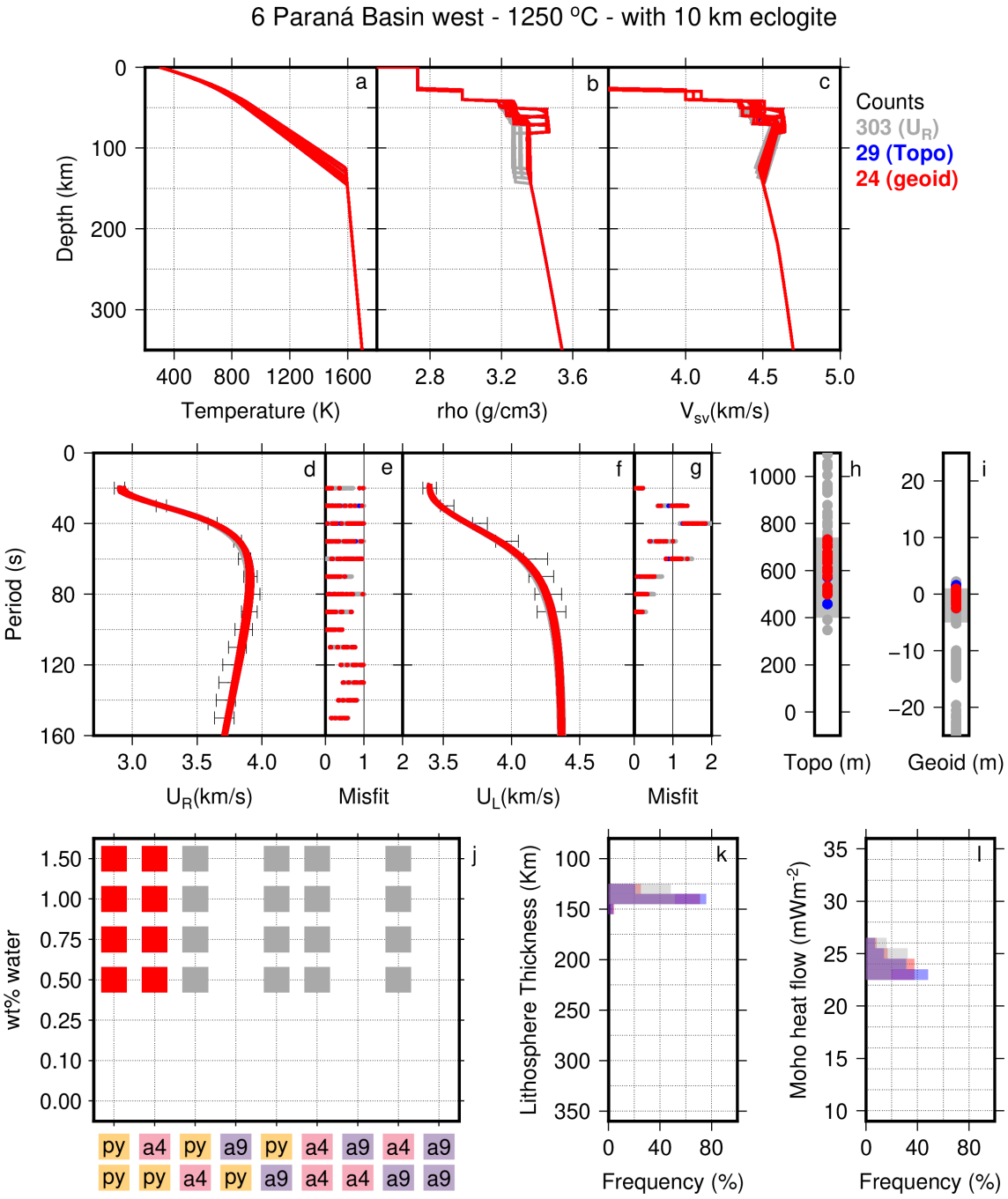

Figure S11 Set of solutions for group 6 Paraná Basin west (6PrB(w)) for a sublithospheric potential temperature of 1250°C with a 10 km eclogitic layer. All solutions that fit the dispersion curves are in grey; those that fit both the dispersion curves and the elevation are in blue; those that fit dispersion curves, elevation, and geoid are in red. Top row: (a) Geotherms, (b) density profiles, and (c) V_{SV} profiles. Middle row: (d) group Rayleigh-wave groups velocities vs period and, (e) respective misfits, (f) group Love-wave groups velocities vs period. and (g) respective misfits, (h) and (i) show elevation and geoid, respectively, with a dark grey box for the observed range. Bottom row: (j) water content vs background composition (top layer/bottom layer), (k) and (l) show histograms of the solutions for thermal lithosphere thickness, and Moho heat flow.

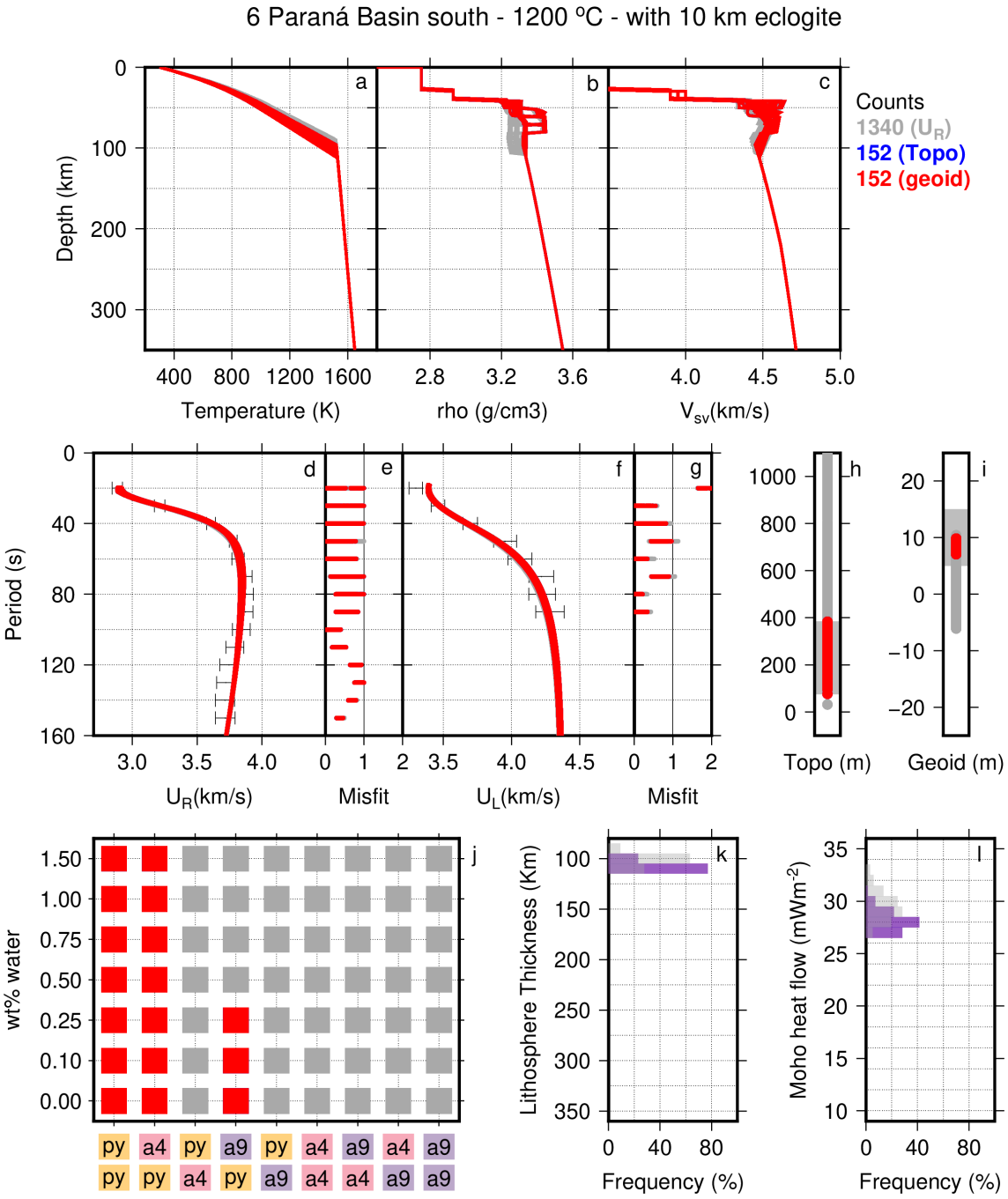

Figure S12 Set of solutions for group 6 Paraná Basin south (6PrB(s)) for a sublithospheric potential temperature of 1200°C with a 10 km eclogitic layer. All solutions that fit the dispersion curves are in grey; those that fit both the dispersion curves and the elevation are in blue; those that fit dispersion curves, elevation, and geoid are in red. Top row: (a) Geotherms, (b) density profiles, and (c) V_{SV} profiles. Middle row: (d) group Rayleigh-wave groups velocities vs period and, (e) respective misfits, (f) group Love-wave groups velocities vs period. and (g) respective misfits, (h) and (i) show elevation and geoid, respectively, with a dark grey box for the observed range. Bottom row: (j) water content vs background composition (top layer/bottom layer), (k) and (l) show histograms of the solutions for thermal lithosphere thickness, and Moho heat flow.

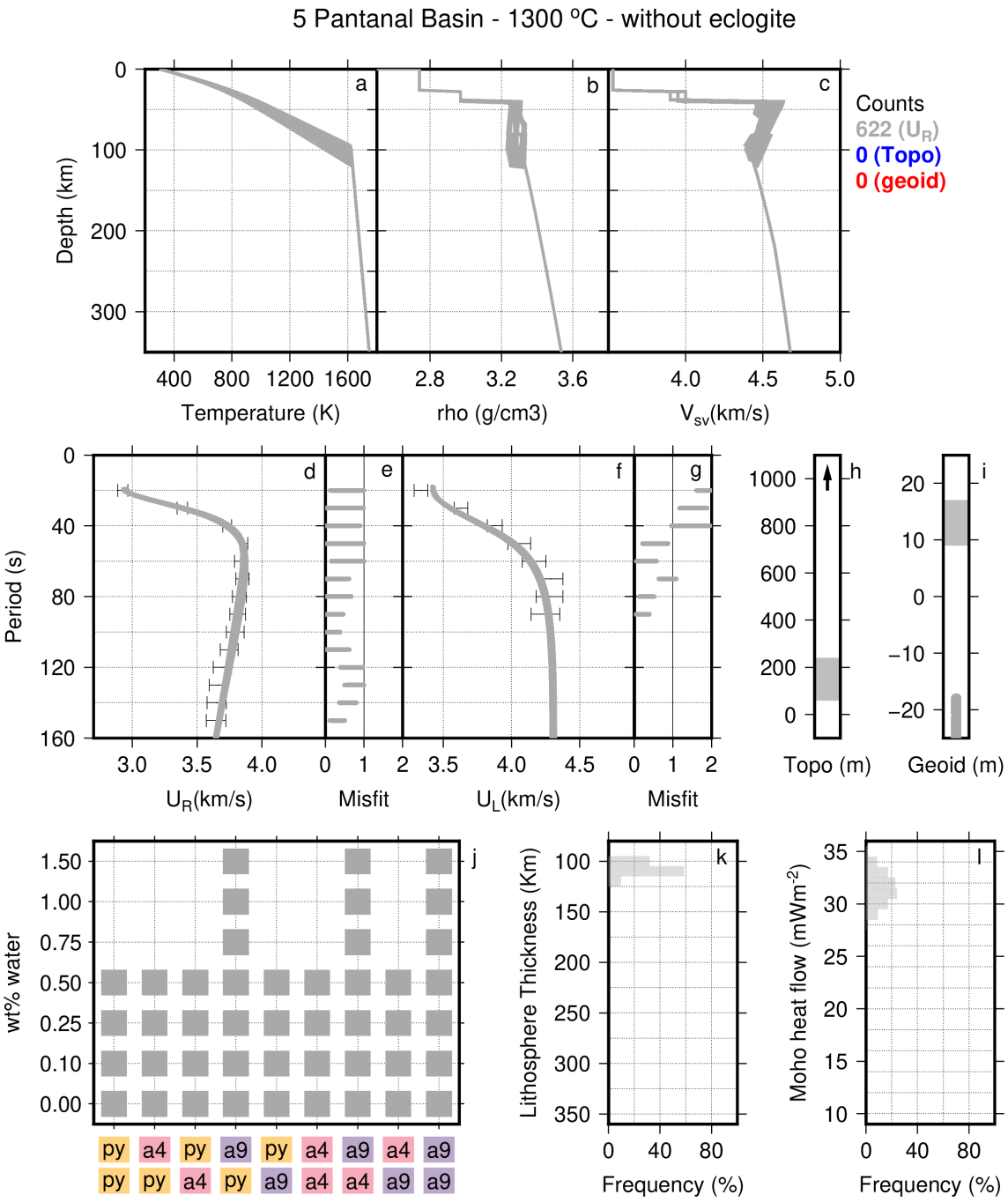

Figure S13 Set of solutions for group 5 Pantanal Basin (5PtB) for a sublithospheric potential temperature of 1300°C without an eclogitic layer. All solutions that fit the dispersion curves are in grey; those that fit both the dispersion curves and the elevation are in blue; those that fit dispersion curves, elevation, and geoid are in red. Solutions for elevation range between 1545 and 3254 meter. Solutions for elevation range between 1545 and 3254 meter. Top row: (a) Geotherms, (b) density profiles, and (c) V_{SV} profiles. Middle row: (d) group Rayleigh-wave groups velocities vs period and, (e) respective misfits, (f) group Love-wave groups velocities vs period. and (g) respective misfits, (h) and (i) show elevation and geoid, respectively, with a dark grey box for the observed range. Bottom row: (j) water content vs background composition (top layer/bottom layer), (k) and (l) show histograms of the solutions for thermal lithosphere thickness, and Moho heat flow.

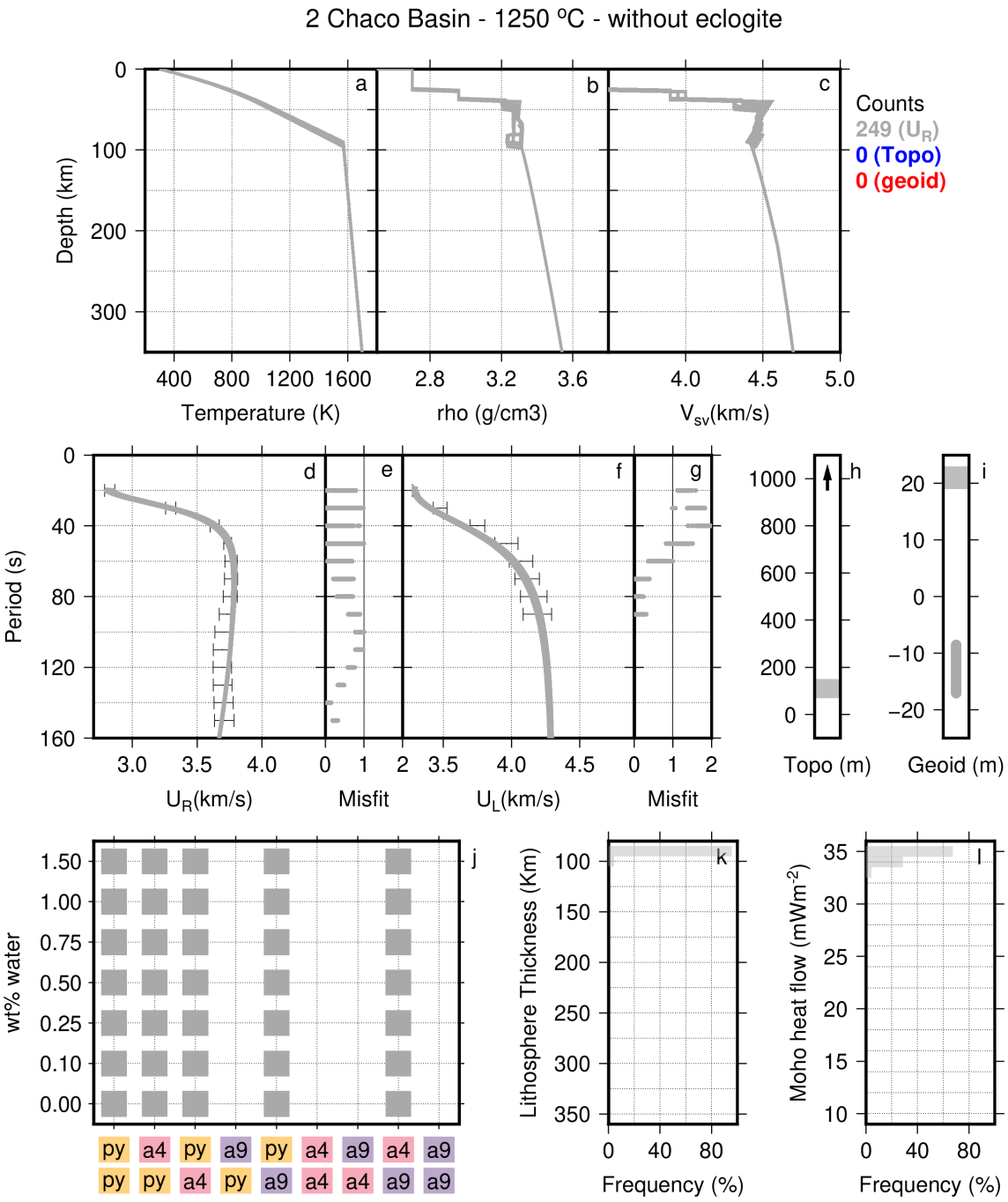

Figure S14 Set of solutions for group 2 Chaco Basin (2ChB) for a sublithospheric potential temperature of 1250°C without an eclogitic layer. All solutions that fit the dispersion curves are in grey; those that fit both the dispersion curves and the elevation are in blue; those that fit dispersion curves, elevation, and geoid are in red. Solutions for elevation range between 1626 and 2564 meters. Top row: (a) Geotherms, (b) density profiles, and (c) V_{SV} profiles. Middle row: (d) group Rayleigh-wave groups velocities vs period and, (e) respective misfits, (f) group Love-wave groups velocities vs period. and (g) respective misfits, (h) and (i) show elevation and geoid, respectively, with a dark grey box for the observed range. Bottom row: (j) water content vs background composition (top layer/bottom layer), (k) and (l) show histograms of the solutions for thermal lithosphere thickness, and Moho heat flow.

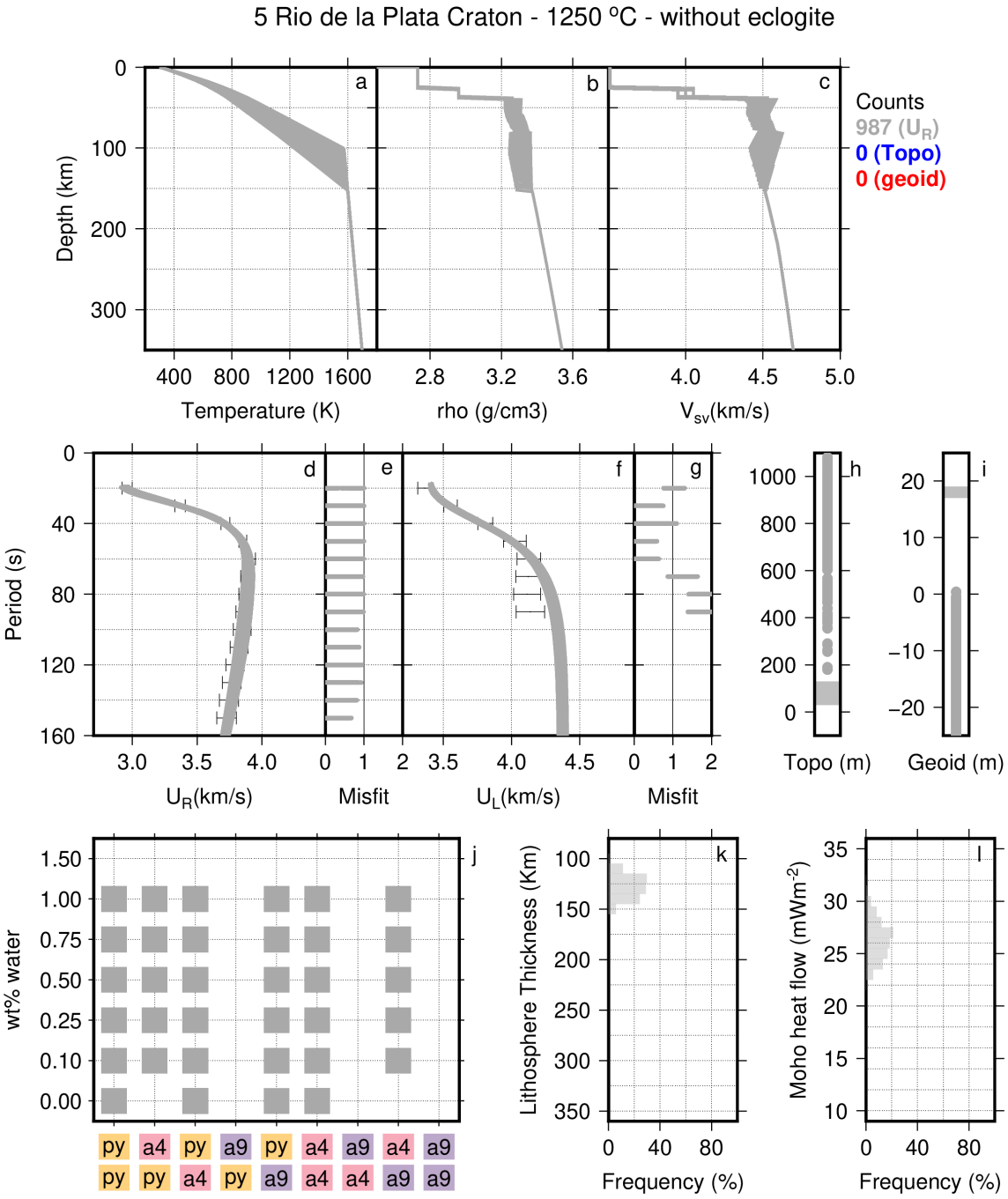

Figure S15 Set of solutions for group 5 Rio de la Plata Craton (5RPC) for a sublithospheric potential temperature of 1250°C without an eclogitic layer. All solutions that fit the dispersion curves are in grey; those that fit both the dispersion curves and the elevation are in blue; those that fit dispersion curves, elevation, and geoid are in red. Top row: (a) Geotherms, (b) density profiles, and (c) V_{SV} profiles. Middle row: (d) group Rayleigh-wave groups velocities vs period and, (e) respective misfits, (f) group Love-wave groups velocities vs period. and (g) respective misfits, (h) and (i) show elevation and geoid, respectively, with a dark grey box for the observed range. Bottom row: (j) water content vs background composition (top layer/bottom layer), (k) and (l) show histograms of the solutions for thermal lithosphere thickness, and Moho heat flow.

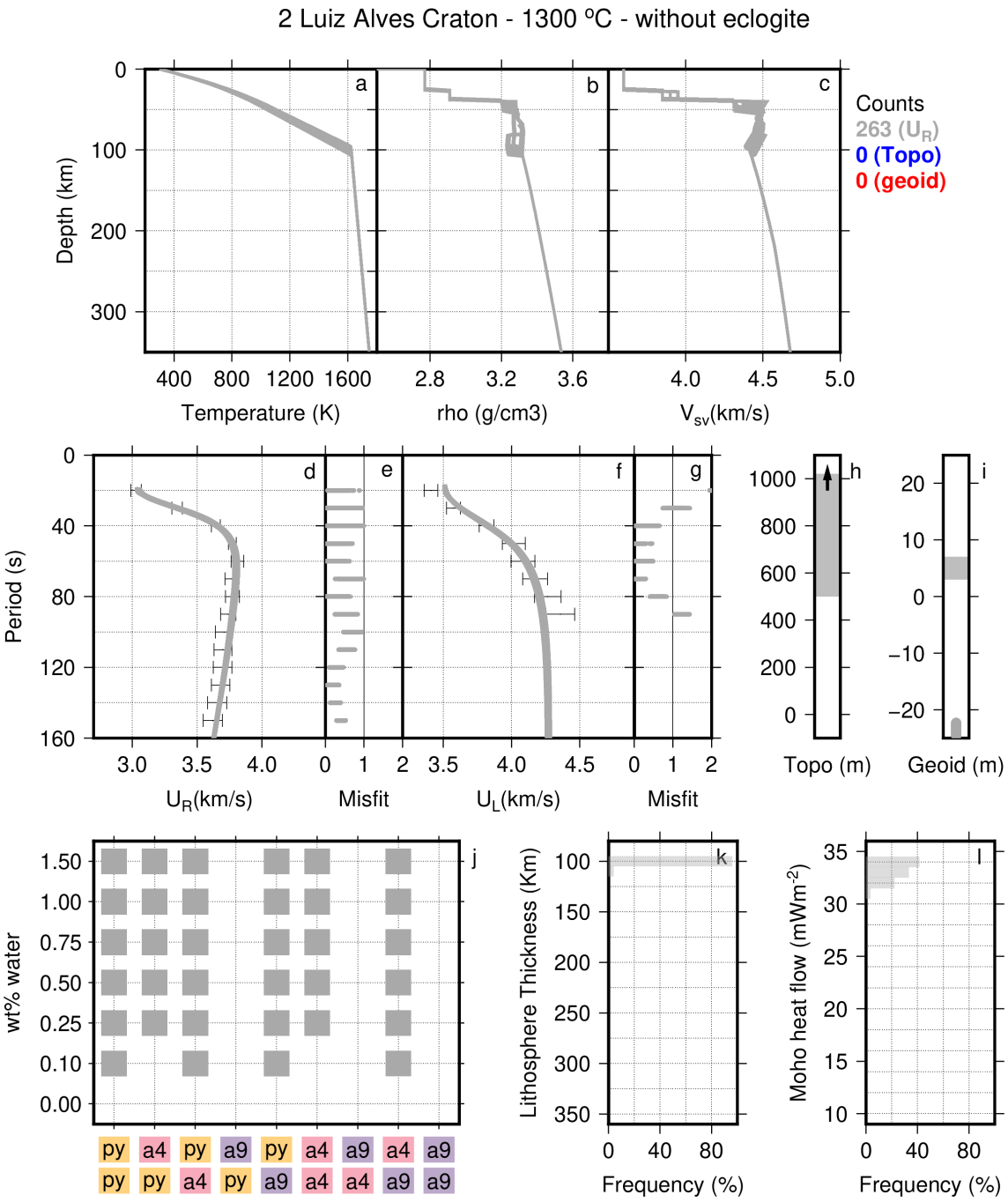

Figure S16 Set of solutions for group 2 Luiz Alves Craton (2LAC) for a sublithospheric potential temperature of 1300°C without an eclogitic layer. All solutions that fit the dispersion curves are in grey; those that fit both the dispersion curves and the elevation are in blue; those that fit dispersion curves, elevation, and geoid are in red. Solutions for elevation range between 1601 and 2838. Top row: (a) Geotherms, (b) density profiles, and (c) V_{SV} profiles. Middle row: (d) group Rayleigh-wave groups velocities vs period and, (e) respective misfits, (f) group Love-wave groups velocities vs period. and (g) respective misfits, (h) and (i) show elevation and geoid, respectively, with a dark grey box for the observed range. Bottom row: (j) water content vs background composition (top layer/bottom layer), (k) and (l) show histograms of the solutions for thermal lithosphere thickness, and Moho heat flow.

References

Griffin, W. L., O'Reilly, S. Y., Afonso, J. C., & Begg, G. C. (2009, 7). The Composition and Evolution of Lithospheric Mantle: a Re-evaluation and its Tectonic Implications. *Journal of Petrology*, *50*(7), 1185–1204. doi: 10.1093/petrology/egn033

Hacker, B. R. (2008, 3). H2O subduction beyond arcs. *Geochemistry, Geophysics, Geosystems*, *9*(3). doi: 10.1029/2007GC001707

Hasterok, D., & Chapman, D. (2011, 7). Heat production and geotherms for the continental lithosphere. *Earth and Planetary Science Letters*, *307*(1-2), 59–70. doi: 10.1016/J.EPSL.2011.04.034

Herzberg, C., Asimow, P. D., Arndt, N., Niu, Y., Lesher, C. M., Fitton, J. G., ... Saunders, A. D. (2007, 2). Temperatures in ambient mantle and plumes: Constraints from basalts, picrites, and komatiites. *Geochemistry, Geophysics, Geosystems*, *8*(2). doi: 10.1029/2006GC001390

Holland, T., Baker, J., & Powell, R. (1998). Mixing properties and activity-composition relationships of chlorites in the system MgO-FeO-Al2O3-SiO2-H2O. *European Journal of Mineralogy*. doi: 10.1127/ejm/10/3/0395

Holland, T., & Powelll, R. (1996). Thermodynamics of order-disorder in minerals: II. Symmetric formalism applied to solid solutions. *American Mineralogist*. doi: 10.2138/am-1996-11-1215

Holland, T. J., & Powell, R. (1998). An internally consistent thermodynamic data set for phases of petrological interest. *Journal of Metamorphic Geology*, *16*(3), 309–343. doi: 10.1111/j.1525-1314.1998.00140.x

Jamieson, H. E., & Roeder, P. L. (1984). The distribution of Mg and Fe2+ between olivine and spinel at 1300oC. *American Mineralogist*, *69*(3-4).

Jaupart, C., & Mareschal, J. C. (1999, 9). The thermal structure and thickness of continental roots. *Lithos*, *48*(1-4), 93–114. doi: 10.1016/S0024-4937(99)00023-7

Laske, G., Masters, G., Ma, Z., & Pasyanos, M. (2013). Update on CRUST1.0—A 1-degree global model of Earth's crust. In *Egu general assembly 2013* (Vol. 15).

Lévy, F., & Jaupart, C. (2011, 1). Temperature and rheological properties of the mantle beneath the North American craton from an analysis of heat flux and seismic data. *Journal of Geophysical Research*, *116*(B1), B01408. doi: 10.1029/2010JB007726

Massonne, H.-J. W. (2008). Phase relations and dehydration behaviour of psammopelite and mid-ocean ridge basalt at very-low-grade to low-grade metamorphic conditions. *European Journal of Mineralogy*. doi: 10.1127/0935-1221/2008/0020-1871

Michaut, C., Jaupart, C., & Bell, D. R. (2007, 4). Transient geotherms in Archean continental lithosphere: New constraints on thickness and heat production of the subcontinental lithospheric mantle. *Journal of Geophysical Research: Solid Earth*, *112*(4). doi: 10.1029/2006JB004464

Newton, R. C., Charlu, T. V., & Kleppa, O. J. (1980). Thermochemistry of the high structural state plagioclases. *Geochimica et Cosmochimica Acta*. doi: 10.1016/0016-7037(80)90283-5

Padrón-Navarta, J. A., Sánchez-Vizcaíno, V. L., Hermann, J., Connolly, J. A., Garrido, C. J., Gómez-Pugnaire, M. T., & Marchesi, C. (2013). Tschermak's substitution in antigorite and consequences for phase relations and water liberation in high-grade serpentinites. *Lithos*. doi: 10.1016/j.lithos.2013.02.001

Rivadeneyra-Vera, C., Bianchi, M., Assumpção, M., Cedraz, V., Julià, J., Rodríguez, M., ... Fernandez, G. (2019). An updated crustal thickness map of central South America based on receiver function measurements in the region of the Chaco, Pantanal, and Paraná Basins, southwestern Brazil. *Journal of Geophysical Research: Solid Earth*, *124*(8), 8491–8505. doi: 10.1029/2018JB016811

Rudnick, R., & Nyblade, A. (1999). The thickness and heat production of Archean lithosphere: constraints from xenolith thermobarometry and surface heat flow. *Mantle petrology: Field observations and high pressure Experimentation: A Tribute to Francis R. (Joe) Boyd*(6), 3–12.

Shapiro, N. M., Ritzwoller, M. H., Mareschal, J. C., & Jaupart, C. (2004, 1). Lithospheric structure of the Canadian Shield inferred from inversion of surface-wave dispersion with thermodynamic a priori constraints. *Geological Society, London, Special Publications*, *239*(1), 175–194. doi: 10.1144/GSL.SP.2004.239.01.12

Wei, C., & Powell, R. (2003). Phase relations in high-pressure metapelites in the system KFMASH (K2O?FeO?MgO?Al2O3?SiO2?H2O) with application to natural rocks. *Contributions to Mineralogy and Petrology*. doi: 10.1007/s00410-003-0454-1

White, Powell, Holland, & Worley. (2000). The effect of TiO2 and Fe2O3 on metapelitic assemblages at greenschist and amphibolite facies conditions: Mineral equilibria calculations in the system K2O-FeO-MgO-Al2O3-SiO2-H2O-TiO2-Fe2O3. *Journal of Metamorphic Geology*. doi: 10.1046/j.1525-1314.2000.00269.x

White, R. W., Powell, R., & Phillips, G. N. (2003). A mineral equilibria study of the hydrothermal alteration in mafic greenschist facies rocks at Kalgoorlie, Western Australia. *Journal of Metamorphic Geology*. doi: 10.1046/j.1525-1314.2003.00454.x

Xu, W., Lithgow-Bertelloni, C., Stixrude, L., & Ritsema, J. (2008). The effect of bulk composition and temperature on mantle seismic structure. *Earth and Planetary Science Letters*, *275*(1-2), 70–79. doi: 10.1016/j.epsl.2008.08.012